J. Mech. Phys. Solids Vol. 29, No. 2, pp. 89–113, 1981.
Printed in Great Britain.

0022–5096/81/020089–25 $02.00/0

AXI-SYMMETRIC CONTACT ON THIN COMPLIANT COATINGS

M. J. MATTHEWSON

University of Cambridge, Department of Physics,
Physics and Chemistry of Solids, Cavendish Laboratory,
Madingley Road, Cambridge CB3 0HE, England

(*Received* 10 *March* 1980)

ABSTRACT

THIS PAPER presents a theory for the indentation of a soft thin coating by a rigid body. The coating is assumed to be bonded to a rigid substrate and to behave linearly elastically. A simplifying approximation enables the stresses within the coating, averaged through its thickness, to be determined for particular indenter profiles. The results are shown to be sensitive to the thickness and compressibility of the coating material. Unlike much previous work, the results can be expressed analytically for certain indenter profiles and have been substantiated by experiment. The theory has many useful applications, in particular for situations where the layer acts as a protective coating and for the accurate, *in situ* and non-destructive measurement of the elastic modulus of the coating material.

NOTATION

a	indenter/coating contact radius
a_H	Hertzian contact radius
h	coating thickness
d	indenter penetration depth
δ	fractional height (in terms of h) of pile-up around the indenter
$f(r)$	function describing the indenter profile
R	spherical indenter radius
θ	cone indenter semi-angle
t	$\tan\theta$
P	load on indenter
P^*	dimensionless load
$u(r, z)$, $v(r, z)$	radial and vertical displacements of the coating
$B(r)$, $C(r)$	functions giving radial dependence of $u(r, z)$
$E(r)$	function giving radial dependence of $v(r, z)$
G, E, ν	elastic constants of the coating material
$\sigma_r, \sigma_\theta, \sigma_z$	normal stresses within the coating; r, θ, z are cylindrical polar coordinates (see Fig. 1)
$\varepsilon_r, \varepsilon_\theta, \varepsilon_z$	corresponding strains
τ_{rz}	radial shear stress, equal to τ_0/τ_1 on lower/upper surface of coating
γ_{rz}	corresponding (engineering) shear strain

The stresses and strains are taken as positive when tensile.

1. INTRODUCTION

THE PROBLEM of contact with a thin soft layer rigidly bonded to a half-space is of great practical interest. Objects are frequently covered by soft layers which can give protection from damage by impact and abrasion or can modify the surface finish. The subject has received much attention in the literature and various analytical approaches have been made.

HANNAH (1951) formulated the problem of the plane-strain contact of a rigid cylinder on an elastic layer in terms of an integral equation. The solution of this equation is complex but has been found for various special cases [see, for example, HANNAH (1951), ALEKSANDROV (1962) and ALEKSANDROV and VOROVICH (1964)]. An analogous integral equation can be derived for axi-symmetric indenters and the solution has been obtained for some special cases [see, for example, SNEDDON (1951)]. However, these methods require sophisticated numerical techniques for determining results which are frequently of an approximate nature and are rarely confirmed by experiment. Further, some techniques are unreliable for coatings whose Poisson's ratio $\nu \gtrsim 0{\cdot}4$. However, MCCORMICK (1978) obtained results for elliptical contact on layers and his results do cover the case of incompressible material, $\nu = 0{\cdot}5$. Dr. J. A. GREENWOOD (Department of Engineering, University of Cambridge) (1979, unpublished work), using a different technique, obtains very close agreement with his work. The work described here will be compared with that of McCormick.

This paper describes an analysis for the contact of an indenter of arbitrary profile with a coating which is rigidly bonded to a semi-infinite substrate. The elastic modulus of the coating is assumed to be small compared with the moduli of the indenter and substrate. The thickness of the coating is assumed to be small compared with the contact radius which in turn is small compared with the characteristic linear dimension of the indenter. Friction between the indenter and coating is ignored.

Using these assumptions, differential equations are found which describe the deformation of the coating. The solution for indentation by a sphere (or paraboloid) is found explicitly for general values of the Poisson's ratio of the coating. A solution for a general indenter profile is found for the case of incompressible material, $\nu = 0{\cdot}5$; and, as an example, indentation by a blunt cone (i.e. a cone with a large semi-angle) is examined. Experiments using spherical and conical indenters show that the results of the analysis are in good agreement with the observed behaviour. The results are also found to agree well with McCormick's work.

The present work was stimulated by experimental studies of the effect of coatings in reducing impact damage, and some reference is made to this problem.

2. ANALYSIS

2.1 *Formulation of the problem*

Figure 1 shows the geometry of the situation. An indenter contacts a coating of thickness h to a depth d with a radius of contact a. The coating piles up around the indenter to a height δh. The movement of the coating material from its unloaded position is described by the vertical and horizontal displacements $v(r, z)$ and $u(r, z)$

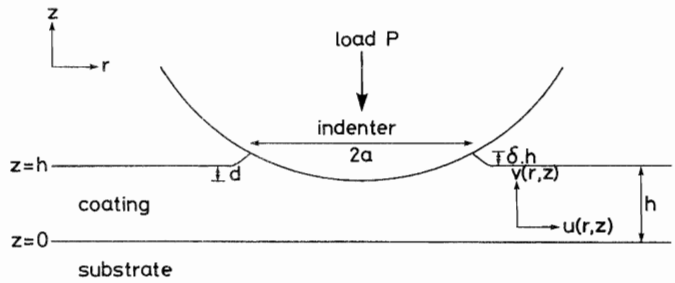

FIG. 1. Geometry of the contact of an indenter with a coated substrate.

(see Fig. 1). The approach adopted here is to seek approximations for these displacements. Having specified forms for the displacements in this way, the four strain components which are non-zero in axial symmetry (ε_r, ε_θ, ε_z, γ_{rz}) may be found (the customary notation is adopted here). However, because of the approximate nature of the displacements, the displacements cannot be made to satisfy exactly the boundary, elasticity and equilibrium conditions at all points in the layer. Because the layer is thin, it is possible to satisfy these conditions to a good approximation with quantities *averaged* through the coating thickness.

The displacements $u(r, z)$ and $v(r, z)$ are approximated by finite power series in z:

$$\left.\begin{aligned} u(r, z) &= A(r)+B(r)z+C(r)z^2,\\ v(r, z) &= D(r)+E(r)z. \end{aligned}\right\}$$

Since $u(r, 0) = v(r, 0) = 0$, because the coating is rigidly attached to the substrate,

$$\left.\begin{aligned} u(r, z) &= B(r)z+C(r)z^2,\\ v(r, z) &= E(r)z, \end{aligned}\right\} \tag{1}$$

where the functions $B(r)$ and $C(r)$ are to be found and $E(r)$ is determined by the indenter profile and penetration of the indenter into the coating. The above approximations can be expected to be good for coatings which are thin compared to the contact radius.

Figure 2 shows the averaged stresses acting on a small element of the coating. Given that $a/h \gg 1$, the radial equilibrium equation becomes

$$\frac{d\bar{\sigma}_r}{dr}+\frac{\bar{\sigma}_r-\bar{\sigma}_\theta}{r}=\frac{\tau_0-\tau_1}{h}, \tag{2}$$

where $\bar{\sigma}_r$ and $\bar{\sigma}_\theta$ are the *averaged* radial and circumferential stresses and τ_0 and τ_1 are the shear stresses acting on the lower and upper surfaces of the coating. Because friction between the indenter and coating is ignored,

$$\tau_1 = 0 \quad \text{for all } r. \tag{3}$$

The radial strain is

$$\varepsilon_r = \frac{\partial u}{\partial r},$$

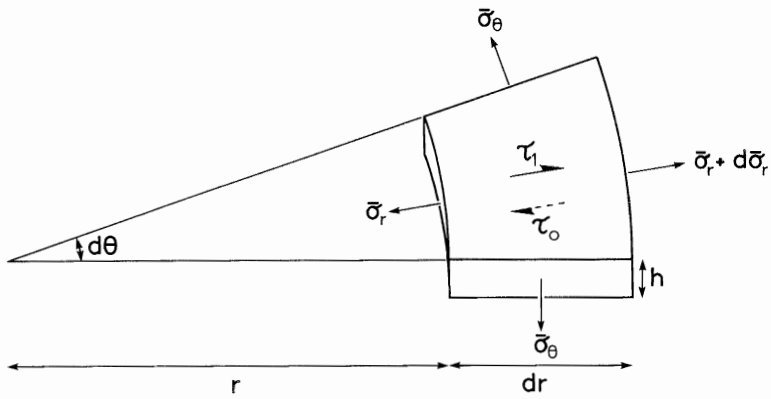

FIG. 2. Stresses acting on a small element of coating.

and using (1),

$$\varepsilon_r = \frac{d}{dr}\{B(r)\}z + \frac{d}{dr}\{C(r)\}^2.$$

The average strain $\bar{\varepsilon}_r$ through the coating thickness is

$$\bar{\varepsilon}_r = \frac{1}{h}\int_0^h \varepsilon_r \, dz,$$

and hence

$$\bar{\varepsilon}_r = \tfrac{1}{2}h\frac{d}{dr}\{B(r)\} + \tfrac{1}{3}h^2\frac{d}{dr}\{C(r)\}. \tag{4}$$

Similarly,

$$\bar{\varepsilon}_\theta = \frac{\bar{u}}{r} = \tfrac{1}{2}h\frac{B(r)}{r} + \tfrac{1}{3}h^2\frac{C(r)}{r} \tag{5}$$

and

$$\bar{\varepsilon}_z = \overline{\frac{\partial v}{\partial z}} = \frac{v(r,h)}{h} = E(r). \tag{6}$$

The elasticity equations for averaged direct stresses and strains are

$$\left.\begin{aligned}
\bar{\sigma}_r &= \frac{2vG}{1-2v}(\bar{\varepsilon}_r + \bar{\varepsilon}_\theta + \bar{\varepsilon}_z) + 2G\bar{\varepsilon}_r, \\
\bar{\sigma}_\theta &= \frac{2vG}{1-2v}(\bar{\varepsilon}_r + \bar{\varepsilon}_\theta + \bar{\varepsilon}_z) + 2G\bar{\varepsilon}_\theta, \\
\bar{\sigma}_z &= \frac{2vG}{1-2v}(\bar{\varepsilon}_r + \bar{\varepsilon}_\theta + \bar{\varepsilon}_z) + 2G\bar{\varepsilon}_z,
\end{aligned}\right\} \tag{7}$$

where v and G are the Poisson's ratio and shear modulus of the coating material. The (engineering) strain is

$$\begin{aligned}
\gamma_{rz} &= \frac{\partial u}{\partial z} + \frac{\partial v}{\partial r} \\
&= B(r) + 2C(r)z + \frac{\partial v(r,z)}{\partial r},
\end{aligned} \tag{8}$$

giving

and from (3),

$$\left.\begin{aligned}\tau_0 &= G(\gamma_{rz})_{z=0} = GB(r),\\ \tau_1 &= G(\gamma_{rz})_{z=h} = 0.\end{aligned}\right\} \tag{9}$$

(i) *Analysis within the contact region* ($r < a$). The averaged strain component $\bar{\varepsilon}_z$ is determined by the shape of the indenter, viz.,

$$\bar{\varepsilon}_z = E(r) = \frac{f(r)}{h} + \delta \tag{10}$$

where $f(r)$ describes the indenter profile. Hence, from (6), (8) and (9),

$$\tau_1 = 0 = G\left\{B(r) + 2hC(r) + \frac{\mathrm{d}f}{\mathrm{d}r}\right\}. \tag{11}$$

Substitution of the strains given by (4), (5) and (10) into the elasticity equations (7) gives the normal stresses in terms of the functions $B(r)$ and $C(r)$. Substitution of the stresses into the equilibrium equation (2), after elimination of the shear stresses τ_0 and τ_1 acting on the coating given by (9), yields

$$\frac{2(1-\nu)}{1-2\nu}\mathscr{D}\{\tfrac{1}{2}hB(r) + \tfrac{1}{3}h^2C(r)\} + \frac{2\nu}{1-2\nu}\frac{1}{h}\frac{\mathrm{d}f}{\mathrm{d}r} = \frac{B(r)}{h}, \quad 0 \leqslant r < a,$$

where $\mathscr{D}$ is the differential operator defined by

$$\mathscr{D}\{g(r)\} = \frac{\mathrm{d}^2 g}{\mathrm{d}r^2} + \frac{1}{r}\frac{\mathrm{d}g}{\mathrm{d}r} - \frac{g}{r^2}.$$

$C(r)$ is eliminated by use of (11), thus yielding a differential equation for $B(r)$:

$$\mathscr{D}\left\{B(r) - \frac{1}{2}\frac{\mathrm{d}f}{\mathrm{d}r}\right\} - \frac{3}{2h^2}\frac{(1-2\nu)}{(1-\nu)}B(r) + \frac{3\nu}{h^2(1-\nu)}\frac{\mathrm{d}f}{\mathrm{d}r} = 0, \quad 0 \leqslant r < a, \tag{12}$$

which, in principle, may be solved for any indenter profile $f(r)$. It is then possible to calculate the stresses and strains from the solution.

(ii) *Analysis outside the contact region* ($r > a$). Equations (8) and $(9)_2$ give

$$B(r) + 2hC(r) + \frac{\mathrm{d}v_1}{\mathrm{d}r} = 0, \tag{13}$$

where $v_1 = v(r, h)$. Now, $\bar{\sigma}_z = 0$ for $r > a$ and therefore from (7),

$$\bar{\varepsilon}_z = -\frac{\nu}{1-\nu}(\bar{\varepsilon}_r + \bar{\varepsilon}_\theta); \tag{14}$$

but $v_1 = h\bar{\varepsilon}_z$ and therefore

$$\frac{\mathrm{d}v_1}{\mathrm{d}r} = -\frac{\nu h}{1-\nu}\left\{\frac{\mathrm{d}\bar{\varepsilon}_r}{\mathrm{d}r} + \frac{\mathrm{d}\bar{\varepsilon}_\theta}{\mathrm{d}r}\right\}. \tag{15}$$

Elimination of (dv_1/dr) from (13) and (15) together with substitution for the strains using (4) and (5) gives

$$\mathscr{D}\{\tfrac{1}{2}hB(r)+\tfrac{1}{3}h^2C(r)\} = \frac{1-\nu}{\nu h}\{B(r)+2hC(r)\}, \quad r > a. \tag{16}$$

Substitution of (14) into (7) followed by substitution into the equilibrium condition (2) with use of (9) gives

$$\mathscr{D}\{\tfrac{1}{2}hB(r)+\tfrac{1}{3}h^2C(r)\} = \frac{1-\nu}{2h}B(r), \quad r > a. \tag{17}$$

Elimination of the left-hand sides of (16) and (17) yields the relation between $B(r)$ and $C(r)$, viz.,

$$C(r) = -\frac{2-\nu}{4h}B(r), \tag{18}$$

which when substituted into (16) or (17) gives

$$\mathscr{D}\{B(r)\} - \frac{6(1-\nu)}{4+\nu}\frac{B(r)}{h^2} = 0, \quad r > a.$$

The general solution of this equation is

$$B(r) = \alpha_1 K_1\left\{\sqrt{\frac{6(1-\nu)}{4+\nu}}\frac{r}{h}\right\} + \alpha_2 I_1\left\{\sqrt{\frac{6(1-\nu)}{4+\nu}}\frac{r}{h}\right\}, \quad r > a,$$

where α_1 and α_2 are disposable constants and $I_1(x)$ and $K_1(x)$ are the first-order modified Bessel functions [see, for example, ABRAMOWITZ and STEGUN (1965)]. Equation (9) shows that $GB(r)$ can be identified with the shear stress acting across the coating/substrate interface. Hence, $B(r)$ must approach zero for large values of r. $I_1(x)$ is bounded for finite $x \geqslant 0$ but unbounded for $x \to \infty$ and hence $\alpha_2 = 0$. This gives

$$B(r) = \alpha_1 K_1\left\{\sqrt{\frac{6(1-\nu)}{4+\nu}}\frac{r}{h}\right\}, \quad r > a. \tag{19}$$

The full solution of the problem will now be found for indentation by a large sphere (Section 2.2) and, when $\nu = \frac{1}{2}$, for a blunt cone (Section 2.3) and an indenter of arbitrary profile (Section 2.4).

2.2 *Solution for indentation by a sphere*

If the radius of the sphere R is much larger than the contact radius a, then the profile of the indenter can be approximated by

$$f(r) = \frac{r^2-a^2}{2R}. \tag{20}$$

Substitution of (20) into (12) gives

$$\mathscr{D}\{B(r)\} - \frac{3(1-2\nu)}{2(1-\nu)}\frac{B(r)}{h^2} + \frac{3\nu r}{(1-\nu)h^2R} = 0, \quad 0 \leqslant r < a.$$

The general solution for $B(r)$ is

$$B(r) = \frac{2\nu}{1-2\nu}\frac{r}{R} + \beta_1 I_1\left\{\sqrt{\frac{3(1-2\nu)}{2(1-\nu)}}\frac{r}{h}\right\} + \beta_2 K_1\left\{\sqrt{\frac{3(1-2\nu)}{2(1-\nu)}}\frac{r}{h}\right\}, \quad 0 \leqslant r < a, \tag{21}_1$$

where β_1 and β_2 are disposable constants. This expression contains two singularities, one at $r = 0$ ($K_1(x)$ is bounded for all $x > 0$ but unbounded at $x = 0$) and another for $v = \frac{1}{2}$, which must be removed since $B(r)$ must be finite. The singularity at the origin $r = 0$ is simply removed by putting $\beta_2 = 0$. The first term is singular for $v = \frac{1}{2}$ and to balance this, β_1 may be chosen so that the second term has a similar singularity and so that the sum of the two remains finite. Evaluation of $B(r)$ with, or near to, $v = \frac{1}{2}$ may then be made by expressing $I_1(x)$ in terms of its analytical power series and combining the diverging linear terms in r to yield an expression which is finite for $0 \leqslant r \leqslant a$ and $-1 \leqslant v \leqslant \frac{1}{2}$ and which *also* satisfies the symmetry condition that the interfacial shear stress is zero at $r = 0$ ($B(0) = 0$), viz.,

$$B(r) = a_1 r + \frac{3(1-2v)a_1 R - 6v}{16(1-v)h^2 R} \sum_{n=1}^{\infty} a_{2n+1} r^{2n+1}, \quad 0 \leqslant r < a, \qquad (21)_2$$

where

$$a_m = \frac{3(1-2v)}{2(1-v)(m^2-1)h^2} a_{m-2}, \quad (m \geqslant 5),$$

$a_3 = 1$, and a_1 is a constant to be found.

The disposable constants α_1, a_1, δ may now be found by suitable matching at the boundary $r = a$. At $r = a$, there are continuity conditions only on the average displacements $\bar{u}, \bar{v}$ (avoiding fracture) and on the stresses $\bar{\sigma}_r, \bar{\tau}_{rz}$ (maintaining equilibrium) but not $\bar{\sigma}_\theta, \bar{\sigma}_z$. This gives *four* conditions but as the theory supplies only *three* disposable constants they cannot all be satisfied and the problem is overdetermined. The "optimum" solution would be to determine the constants by an energy method, which is straightforward. However, here, an *empirical* procedure of imposing continuity on the three normal strains (or, equivalently, stresses) is adopted, this being justified *post hoc* in terms of the agreement between the theoretical results thereby predicted and both the experimental results and predictions of the work of McCormick (1978) (Section 3). The reason for the apparent success of this method is not entirely clear and is a subject for further work. The inconsistency involved in the theory leads to some error in the results which manifests itself in a few per cent mismatch in $\bar{\tau}_{rz}$ at $r = a$.

The analytical expression for a_1 is non-trivial but the expressions for α_1 in (19), β_1 in (21) and δ are readily found:

$$\left.\begin{aligned} \beta_1 &= \frac{(K'a-K)(1-6v)}{(KI'-IK')(1-2v)2R}, \\ \alpha_1 &= \frac{-4}{(4+v)K'}\left\{\frac{1-6v}{2(1-v)R} + \beta_1 I'\right\}, \\ \delta &= -\frac{v}{1-v}\frac{4+v}{12}\frac{h}{a}\alpha_1(K'a+K), \end{aligned}\right\}$$

where

$$\left.\begin{aligned} I &= I_1\left\{\sqrt{\frac{3(1-2v)}{2(1-v)}}\frac{a}{h}\right\}, \quad I' = \frac{\mathrm{d}I}{\mathrm{d}a}, \\ K &= K_1\left\{\sqrt{\frac{6(1-v)}{4+v}}\frac{a}{h}\right\}, \quad K' = \frac{\mathrm{d}K}{\mathrm{d}a}. \end{aligned}\right\}$$

Examination of these results shows that all stresses and strains are inversely proportional to the indenter radius R. Therefore, the stresses and strains will be scaled by the dimensionless factor R/a in the figures. When presented in this way, these quantities are only functionally dependent on a/h and ν.

(i) *Alternative solution for* $\nu = \frac{1}{2}$. In practical circumstances, it is found that *elastomeric coatings* are very much more successful than other materials for protecting components from impact damage. For this reason, the experiments described in this paper have been confined to *nearly incompressible materials*. Numerical evaluation of the stress distribution in this case poses an apparent problem as (7) contains terms which become a ratio of infinitesimals as $\nu \to \frac{1}{2}$. The stress distribution can be obtained using the above theory when ν is very close to $\frac{1}{2}$, but a simplified solution may be found when $\nu = \frac{1}{2}$ precisely and this is described here.

When $\nu = \frac{1}{2}$, the solution for the function $B(r)$ reduces to

$$B(r) = \begin{cases} \beta_3 \dfrac{r}{a} + \dfrac{3a^3}{8h^2R}\left[1 - \left(\dfrac{r}{a}\right)^2\right]\left(\dfrac{r}{a}\right), & 0 \leqslant < a, \\ \alpha_1 K_1\left(\sqrt{\dfrac{2}{3}}\,\dfrac{r}{h}\right), & r > a. \end{cases} \tag{22}$$

The strains are given by

$$\left.\begin{aligned} \bar{\varepsilon}_r &= \frac{h\beta_3}{3a} + \frac{a^2 - 3r^2}{8Rh} - \frac{h}{6R}, \\ \bar{\varepsilon}_\theta &= \frac{h\beta_3}{3a} + \frac{a^2 - r^2}{8Rh} - \frac{h}{6R}, \\ \bar{\varepsilon}_z &= \frac{r^2 - a^2}{2Rh} + \delta, \end{aligned}\right\} \quad 0 \leqslant r < a,$$

$$\left.\begin{aligned} \bar{\varepsilon}_r &= \frac{3}{8} h\alpha_1 \frac{\mathrm{d}}{\mathrm{d}r}\left\{K_1\left(\sqrt{\frac{2}{3}}\,\frac{r}{h}\right)\right\}, \\ \bar{\varepsilon}_\theta &= \frac{3}{8} h\alpha_1 \frac{1}{r} K_1\left(\sqrt{\frac{2}{3}}\,\frac{r}{h}\right), \\ \bar{\varepsilon}_z &= -(\bar{\varepsilon}_r + \bar{\varepsilon}_\theta), \end{aligned}\right\} \quad r > a, \tag{23}$$

which, when matched at $r = a$, give

$$\left.\begin{aligned} \alpha_1 &= \frac{2a^3}{3h^2R(K - K'a)}, \\ \beta_3 &= \frac{9\alpha_1 K}{8} + \frac{a}{2R}, \\ \delta &= \frac{a^2}{4Rh} + \frac{h}{3R} - \frac{2h\beta_3}{3a}. \end{aligned}\right\}$$

Equations (7) reduce to

$$\left.\begin{aligned}\bar{\sigma}_r &= \bar{\sigma}_0 + 2G\bar{\varepsilon}_r,\\ \bar{\sigma}_\theta &= \bar{\sigma}_0 + 2G\bar{\varepsilon}_\theta,\\ \bar{\sigma}_z &= \bar{\sigma}_0 + 2G\bar{\varepsilon}_z,\end{aligned}\right\} \tag{24}$$

when $\nu = \frac{1}{2}$, where $-\bar{\sigma}_0$ is the averaged hydrostatic pressure. Now, $\bar{\sigma}_z = 0$ and $\bar{\varepsilon}_z = \delta$ at $r = a$, and from (24),

$$\bar{\sigma}_0 = -2G\delta \quad \text{at } r = a. \tag{25}$$

A differential equation for $\bar{\sigma}_0$ is obtained by substituting (23) and (24) into the equilibrium equation (2). When this is solved, with use of (25) as a boundary condition, $\bar{\sigma}_0$ is obtained as

$$\frac{\bar{\sigma}_0}{G} = (r^2 - a^2)\left[\frac{\beta_3}{2ah} + \frac{1}{hR} - \frac{3}{32h^3R}(r^2 - a^2)\right] - 2\delta,$$

and hence the normal stresses may be obtained. The total compression load P can now be found by integrating $\bar{\sigma}_z$ over the contact area, viz.,

$$P = \pi a^2 G\left(\frac{a\beta_3}{4h} + \frac{a^2}{hR} + \frac{a^4}{32h^3R}\right). \tag{26}$$

This special solution ($\nu = \frac{1}{2}$) is indistinguishable from the general solution ($0 \leqslant \nu < \frac{1}{2}$) when $\nu = 0{\cdot}49999$, and therefore it provides both a check for the analysis and a simpler representation of the solution for incompressible coating materials.

(ii) *Results.* The stress distributions have been found to be very sensitive to the compressibility of the coating. Figure 3(a) shows the distribution of the interfacial shear stress τ_0 with radius r for various values of ν. The results are calculated for $a/h = 5$. The magnitude of τ_0 rises rapidly as the coating becomes less compressible ($\nu \to \frac{1}{2}$). This may be interpreted physically in the following terms. The coating material volume must be removed from beneath the indenter. This is achieved in two ways; firstly, by compression of the coating; and secondly, by radial movement of material away from the contact zone. For virtually incompressible coatings, the first mechanism is negligible and thus the radial movement is greater in this case. The shear stress on the interface is a result of this radial displacement. The sensitivity of τ_0 to Poisson's ratio is of practical significance as protective coatings are frequently highly incompressible elastomers and are shown here to be more vulnerable to debonding than other materials with similar elastic moduli. Debonding of protective coatings is undesirable.

Figure 3(b) shows the radial distribution of τ_0 for various coating thicknesses

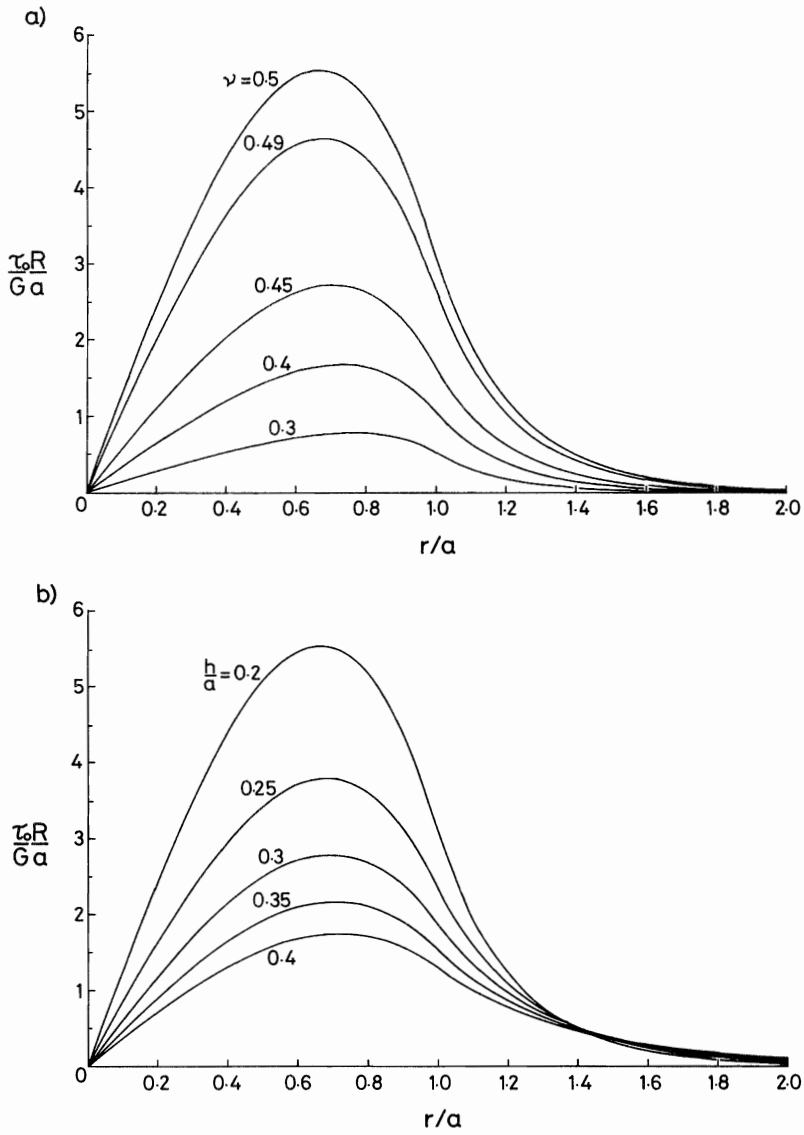

FIG. 3. Indentation by a sphere. The variation of the coating/substrate interfacial shear stress τ_0 with radius for various values of (a) Poisson's ratio of coating ν and (b) coating thickness h/a. The results are calculated for (a) $a/h = 5$ and (b) $\nu = 0{\cdot}5$.

calculated for $\nu = \frac{1}{2}$. The magnitude of τ_0 rises rapidly as the thickness decreases.

Figure 4 shows the radial distributions of the averaged direct stresses and strains calculated for $a/h = 5$ and various values of ν. All the stresses and strains are sensitive to ν. A large hydrostatic pressure is developed beneath the indenter and this results in the three normal stresses being compressive everywhere, despite the fact that $\bar{\varepsilon}_r$ and $\bar{\varepsilon}_\theta$ are tensile around $r = 0$.

Figure 5 shows the variation of a/a_H with a_H/h for $\nu = 0{\cdot}5$ for both the present and

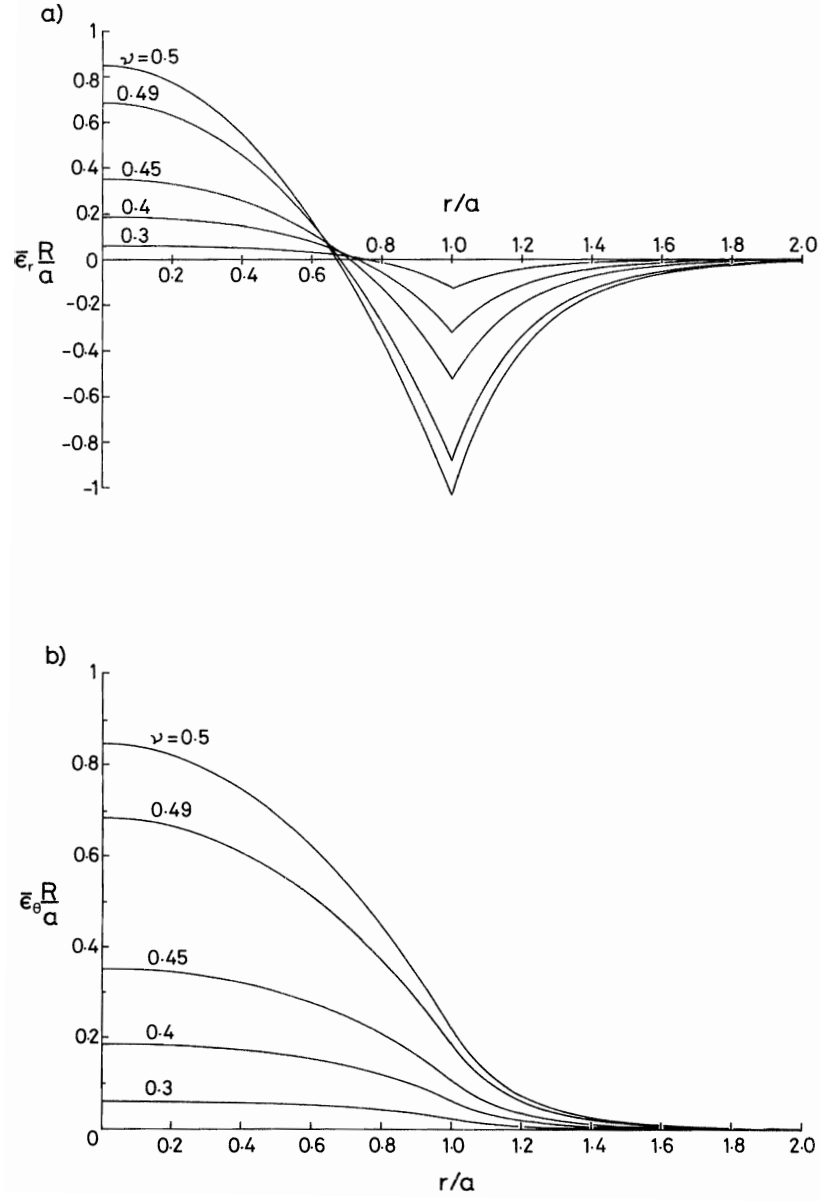
a)
$\bar{\epsilon}_r \frac{R}{a}$
r/a
ν=0·5
0·49
0·45
0·4
0·3
b)
$\bar{\epsilon}_\theta \frac{R}{a}$
r/a
ν=0·5
0·49
0·45
0·4
0·3

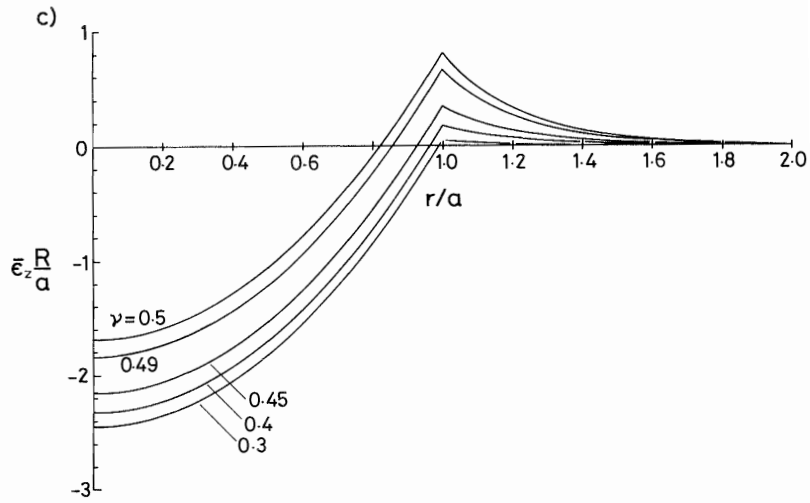
c)
1
0
-1
-2
-3
0·2
0·4
0·6
1·0
1·2
1·4
1·6
1·8
2·0
r/a
$\bar{\epsilon}_z \frac{R}{a}$
ν=0·5
0·49
0·45
0·4
0·3

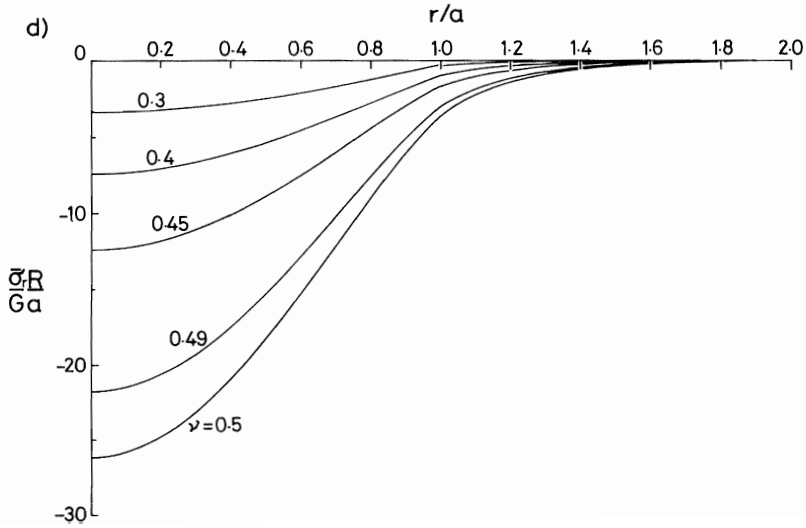
d)
r/a
0
0·2
0·4
0·6
0·8
1·0
1·2
1·4
1·6
1·8
2·0
-10
-20
-30
$\frac{\bar{\sigma}_r R}{Ga}$
0·3
0·4
0·45
0·49
ν=0·5

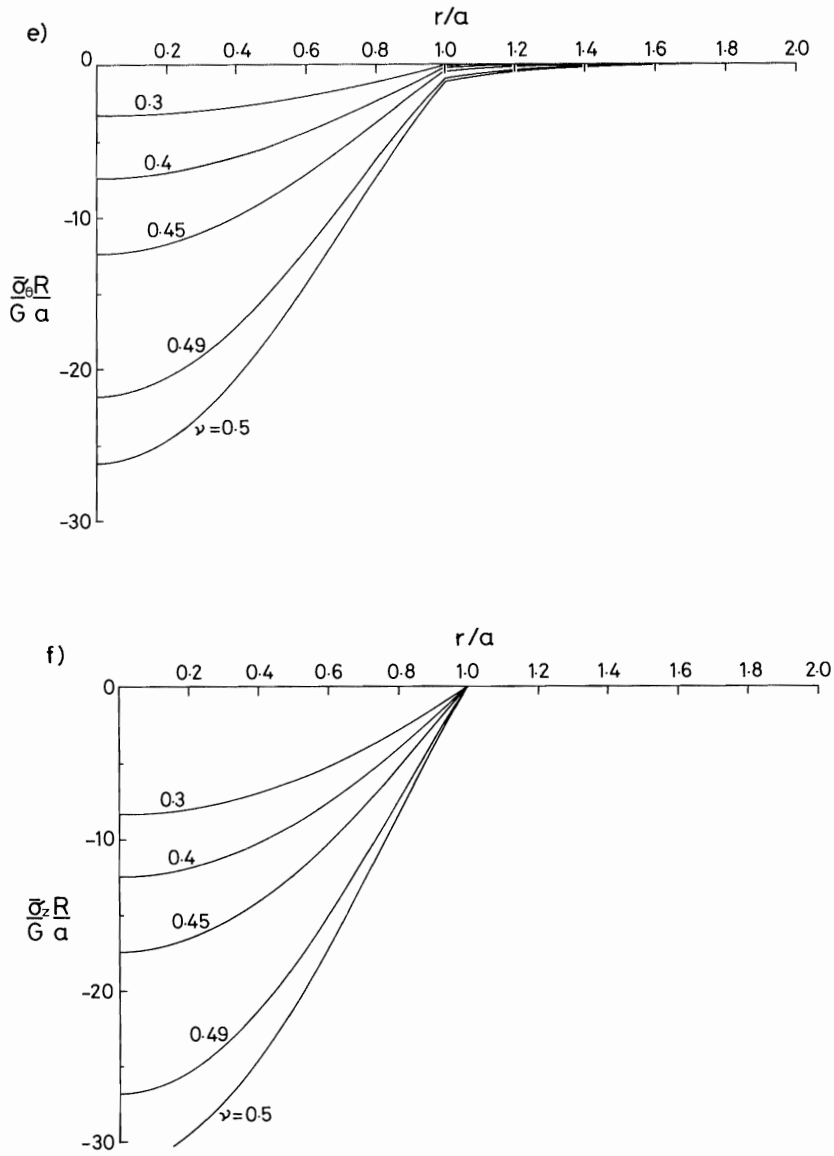

FIG. 4. Indentation by a sphere. The variation of normal stresses and strains (averaged through the coating thickness) with radius for various values of ν: (a) $\bar{\varepsilon}_r$, (b) $\bar{\varepsilon}_\theta$, (c) $\bar{\varepsilon}_z$, (d) $\bar{\sigma}_r$, (e) $\bar{\sigma}_\theta$, (f) $\bar{\sigma}_z$. Results are calculated for $a/h = 5$.

McCORMICK's (1978) theories. Here, a_H is the Hertzian contact radius for contact on a coating of infinite thickness, viz.,

$$a_H = \left(\frac{3PR(1-\nu)}{8G}\right)^{1/3}.$$

In this form, the result is a "master-curve" for this particular value of ν. In reality, the ordinates of the curve should approach unity for small a/h but, due to the approximations made in the present analysis, this is not so. The analysis will therefore only be a good description of the contact for $a/h \gtrsim 2$.

2.3 *Solution for indentation by a cone*

The profile function $f(r)$ for a conical indenter is

$$f(r) = \frac{r-a}{\tan\theta}, \tag{27}$$

where θ is the cone semi-angle. The analysis will only be valid for blunt cones with $\tan\theta \gg 1$.

Substitution of (27) into (12) gives

$$\mathscr{D}\{B(r)\} - \frac{3}{2h^2}\frac{1-2\nu}{1-\nu}B(r) + \frac{3\nu}{h^2(1-\nu)t} + \frac{1}{2tr^2} = 0, \quad 0 \leqslant r < a,$$

where $t = \tan\theta$. A simple solution for $B(r)$ may be found only for $\nu = \frac{1}{2}$, viz.,

$$B(r) = \beta_4 r + \frac{\beta_5}{r} + \frac{1}{2t} - \frac{r^2}{h^2 t}, \quad 0 \leqslant r < a,$$

$\beta_5 = 0$, given that $B(r)$ is finite at $r = 0$. $B(r)$ is discontinuous at the origin and this results from the discontinuous nature of the indenter profile. However, the discontinuity is small and the displacement $\bar{u}(0) = 0$ so that there is no material discontinuity even though $\tau_0(0) \neq 0$. The stress distributions may be found in a manner parallel to that used for the special case of a spherical indentation when $\nu = \frac{1}{2}$. The solution outside the contact region, $r > a$, is unchanged [equation (19)].

The strains within the contact region are given by

$$\left.\begin{aligned} \bar{\varepsilon}_r &= \frac{h}{3}\left(\beta_4 - \frac{2r}{h^2 t}\right), \\ \bar{\varepsilon}_\theta &= \frac{h}{3}\left(\beta_4 - \frac{r}{h^2 t}\right), \\ \bar{\varepsilon}_z &= \frac{r-a}{ht} + \delta, \end{aligned}\right\} \quad 0 \leqslant r < a,$$

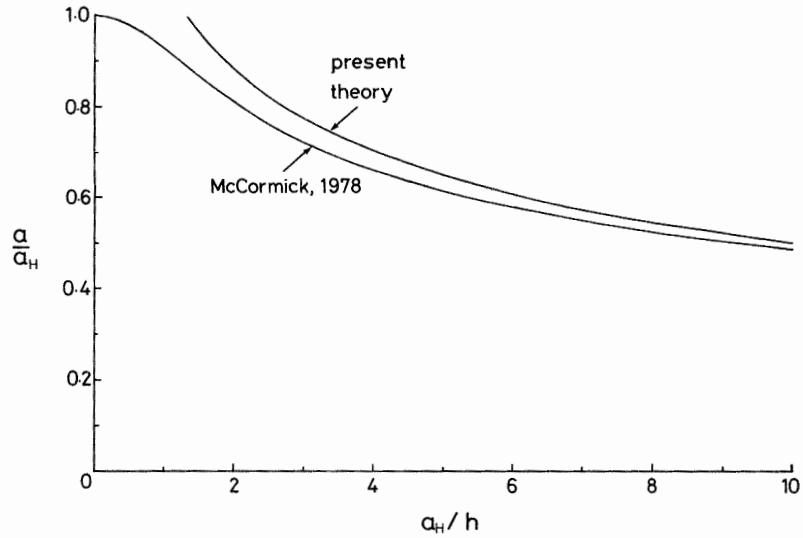

FIG. 5. Indentation by a sphere. Variation of a/a_H with a_H/h for $\nu = 0{\cdot}5$ according to the present theory and McCORMICK's (1978) theory.

and on matching strains at $r = a$ the constants are found as

$$\left.\begin{aligned} \alpha_1 &= \frac{8a^2}{9h^2t(K-K'a)}, \\ \beta_4 &= \frac{9\alpha_1 K}{8a} + \frac{a}{h^2t}, \\ \delta &= \frac{a}{ht} - \frac{2\beta_4 h}{3}. \end{aligned}\right\}$$

The total load is given by

$$P = \pi a^2 G\left(\frac{3a}{2ht} + \frac{\beta_4 a^2}{4h} - \frac{a^3}{5h^3t}\right).$$

2.4 *Solution for general indenter profile*

The solution of (12) for a general indenter profile is not simple for $\nu \neq \frac{1}{2}$. However, for $\nu = \frac{1}{2}$ a simple solution for $B(r)$ in terms of a power series in r can be found. It is assumed, of course, that there is complete contact between the indenter and coating in the region $0 \leqslant r \leqslant a$.

If the indenter profile is expressed by a power series

$$f(r) = \sum_{n=0}^{\infty} b_n r^n,$$

then $B(r)$ may be expressed as

$$B(r) = \sum_{n=0}^{\infty} c_n r^n.$$

On substitution into (12) the coefficients of r^n may be equated and $B(r)$ is given by

$$B(r) = \tfrac{1}{2}b_1 + \beta_6 r + \sum_{n=2}^{\infty} \left\{ \tfrac{1}{2}(n+1)b_{n+1} - \frac{3}{h^2(n+1)} b_{n-1} \right\} r^n,$$

where β_6 is a disposable constant. The general solution of $B(r)$ outside the contact region is independent of the indenter profile and is therefore given by (19). Hence, the stresses within the coating can be found for any indenter where the profile may be expressed by an analytical power series in r.

3. Experimental

3.1 *Indentation by spheres*

Before proceeding to describe the experimental results it is useful to discuss the range for which the present theory will be accurate.

(i) *Region of validity*. It has been assumed that the indenter and substrate are rigid. A correction can be made if small displacements are involved. It is assumed that the $\bar{\sigma}_z$-distribution approximates the "semi-elliptical" distribution for the contact stress of the Hertzian analysis for the contact of two curved surfaces. We now denote the Poisson's ratios and shear moduli of the indenter and substrate by ν_i, ν_s, G_i, G_s. Hertzian theory predicts that the change in curvature of the indenter for the indenter/coating contact is given by

$$\kappa_i = \frac{3P}{4a^3} \frac{1-\nu_i}{2G_i},$$

and similarly for the indenter/substrate contact,

$$\kappa_s = \frac{3P}{4a^3} \frac{1-\nu_s}{2G_s},$$

so that the coating is confined between an effective curvature $(1/R')$ given by

$$\frac{1}{R'} = \frac{1}{R} + \kappa_s - \kappa_i,$$

i.e.

$$\frac{R}{R'} = 1 - \frac{3PR}{4a^3} \left\{ \frac{1-\nu_i}{2G_i} + \frac{1-\nu_s}{2G_s} \right\}. \tag{28}$$

This correction can readily be applied as the stress and strain distributions are inversely proportional to the indenter radius. Clearly, the analysis breaks down if this correction deviates significantly from unity.

It is assumed that the indenter radius is large compared with the contact radius and therefore that the indenter is approximately paraboloidal. As the stresses are inversely proportional to the indenter radius, a certain error in the indenter profile will produce an accumulative error in the stresses across the contact region. If the error in the profile is to be less than 1%, then

$$\frac{a}{R} \lesssim 0{\cdot}2. \tag{29}$$

The coating thickness has been assumed to be small compared with the contact radius, but as the thickness increases, the situation approaches Hertzian contact of the indenter on *bulk* coating material. Figure 5 compares the predictions of the present theory for the variation of a/a_H with a_H/h with McCormick's (1978) result. a_H is the Hertzian contact radius for indentation on bulk coating material with the same load. Examination of this diagram shows that, assuming McCormick's predictions to be accurate, the present theory becomes increasingly accurate with increasing a/h and is better than

$$10\% \quad \text{for } a/h > 2 \quad \text{and} \quad 3\% \text{ for } a/h > 5. \tag{30}$$

Hertzian theory will be valid for $a/h \lesssim 1$.

Linear elasticity has been assumed throughout but is only valid for small strains. The maximum strain is $\bar{\varepsilon}_z$ at $r = a$ and is given by

$$\bar{\varepsilon}_z = -\frac{a^2}{2Rh} + \delta.$$

However, $\bar{\varepsilon}_z$ falls off quite rapidly with radius and large strains are localized at the origin. Therefore, a large strain can be tolerated here. If the strain is limited to 20%, then

$$\frac{a^2}{R^2} < 0{\cdot}6\,\frac{h}{R}, \tag{31}$$

given that δ is approximately $a^2/6Rh$ for elastomeric coatings. For other materials which may fail under shear at strains much less than 20%, a more rigid condition should be imposed. Equations (29)–(31) define regions in an $(h/R, a/R)$-plane over which the analysis can be expected to be valid. Figure 6 shows regions A where better than 10% accuracy is achieved, B where the error is less than 3%. In region C, Hertzian theory will be a good approximation.

(ii) *Apparatus.* Figure 7 shows the apparatus used to verify the analysis of Section 3. Weights are used to load a spherical indenter onto a coating which is attached to a glass slab. The glass has an abraded surface to give a good non-slipping adhesion with the coating. Ink containing detergent is placed between the glass indenter and coating in order to provide both lubrication and good visibility of the edge of the contact. The contact radius is measured by direct viewing from underneath using a travelling microscope. A dial gauge attached to the loading apparatus gives a direct reading of the penetration of the indenter. Silicone rubber was used as the coating material as it is transparent and can readily be cast in a liquid form to any required thickness. The

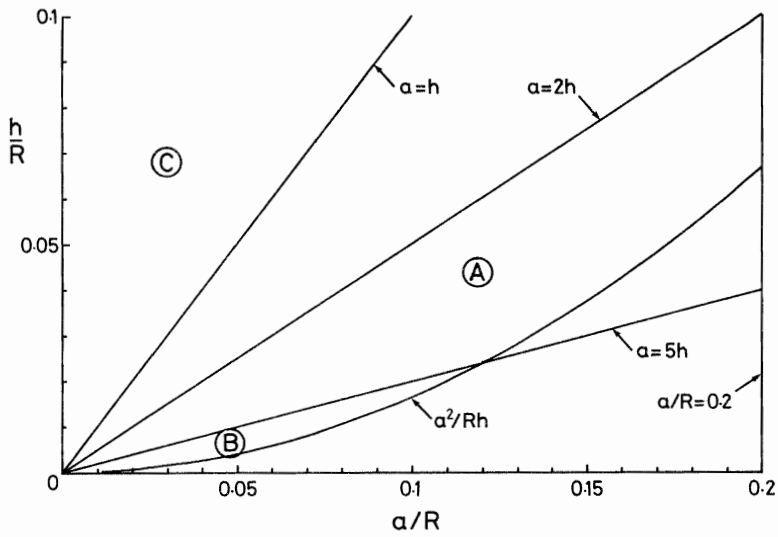

FIG. 6. Indentation by a sphere. Regions of validity for the theory in the $(h/R, a/R)$-plane. Region A is better than 10% and B better than 3%.

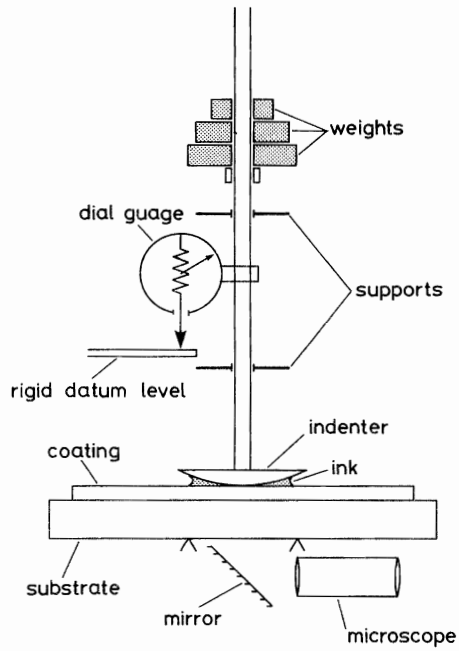

FIG. 7. Experimental apparatus for measuring contact radius and penetration as a function of the applied load.

elastic modulus of the rubber is more than four orders of magnitude less than the moduli of the indenter and substrate and the correction term of (28) does not differ significantly from unity. The modulus of the coating varies between specimens and with time, and it was measured for each specimen individually by hanging weights on a strip of detached coating and measuring a gauge length as a function of load. The maximum strains involved were large (up to 10%) and the modulus was estimated from true stress vs true strain graphs to an accuracy of typically 5%.

Both the contact radius a and penetration d have been measured as a function of load P and the total region defined in Fig. 6 has been systematically explored.

(iii) *Load vs contact radius results.* Figure 8(a) shows the results of measurements of the contact radius as a function of applied load. The behaviour predicted by the

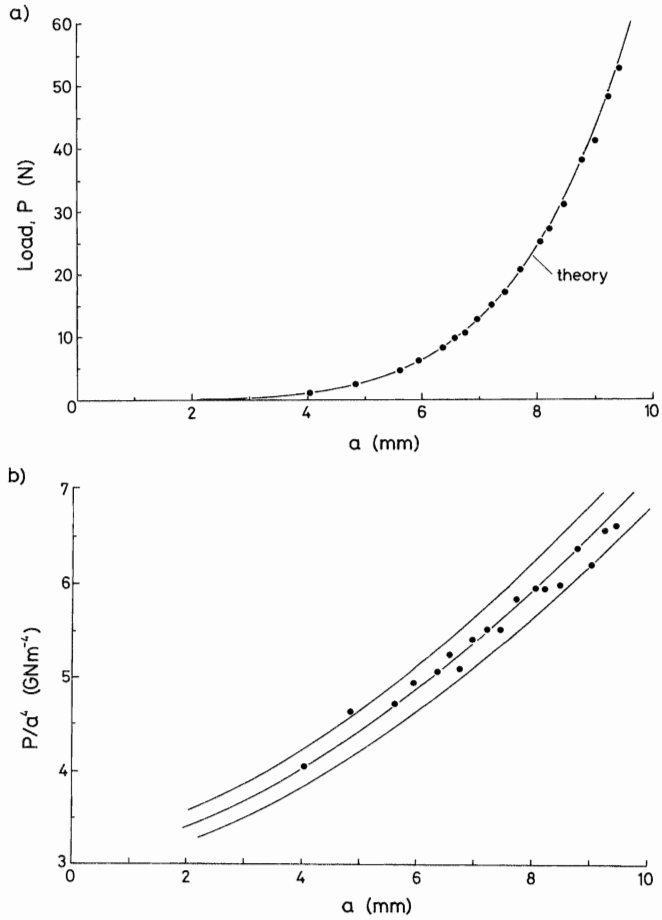

FIG. 8. Indentation by a sphere. (a) Variation of load P with contact radius a. The theory-line is calculated using the measured values $G = 89$ kPa, $R = 47$ mm, $h = 2{\cdot}15$ mm and $\nu = 0{\cdot}5$. (b) Results of (a) replotted as P/a^4 vs a. The three theory-lines are calculated using the measured value of the elastic modulus and this value plus and minus the error of 5%.

theory is shown and is calculated using the measured values of $h = 2{\cdot}15$ mm, $R = 47$ mm and $G = 89$ kPa. The fit is extremely good. It should be noted that the theory-line and experimental points are entirely independent. The degree of fit is shown better in Fig. 8(b). The error in the data-points is predominantly in the contact radius. By plotting P/a^4 vs a the data are spread out by artificially introducing scatter into the ordinates. The three theory-lines are calculated for the modulus equal to its mean value and this value plus and minus the error of 5%. There is no significant systematic deviation of the theory from the data, which shows that although the theory deviates from McCORMICK's (1978) results, the form of the curve is extremely close to the observed behaviour. Further, the scatter in the data is less than the error in the modulus. Thus, an estimate of the modulus with a *random* error of appreciably less than 5% can be made by fitting the theory directly to the data and very small differences in modulus can be resolved. This technique is therefore useful for making *in situ* non-destructive modulus measurements on soft coatings.

Figure 9 shows the predictions of the present and McCormick's theories for the variation of a/a_H with a_H/h for $\nu = 0{\cdot}5$. The lines represent "master-curves" for the behaviour of all materials of this value of Poisson's ratio. In essence, these curves give the variation of contact radius with load, but when plotted in this form the contact radius can be found from the applied load, which is the more usual requirement of such a theory. Superimposed upon these curves are data from several experiments for various values of G, R, h. The data confirm the validity of both the theories within the expected limits.

(iv) *Load vs penetration results.* The penetration d (see Fig. 1) of the indenter into the coating is given by

$$d = -h\bar{\varepsilon}_{z\,(r=0)} = \frac{a^2}{2R} - \delta \,.\, h.$$

Figure 10(a) shows typical results of measurements of d as a function of load. The open circles are the data-points as measured in the experiment. The theory-line is calculated for $G = 24$ kPa, $b = 2{\cdot}88$ mm and $R = 47$ mm. The data are shifted horizontally from the theory-line. By adding 90 μm to the measured values of d much better agreement between theory and experiment is achieved (solid circles). This offset is due to the error in estimating the height at which the indenter just makes contact with the coating.

To examine the fit, the modified data-points are replotted in Fig. 10(b) as P/d^3 vs d. There is little systematic difference between theory and experiment and the predictions of the theory are confirmed.

It has been found that the point at which the indenter first contacts the coating is extremely difficult to observe. Because the penetration varies rapidly with load at this point any error in this datum level will be extremely significant. Therefore, measurement of the penetration as a function of load is not as convenient a method for estimating the coating modulus as measuring the contact radius.

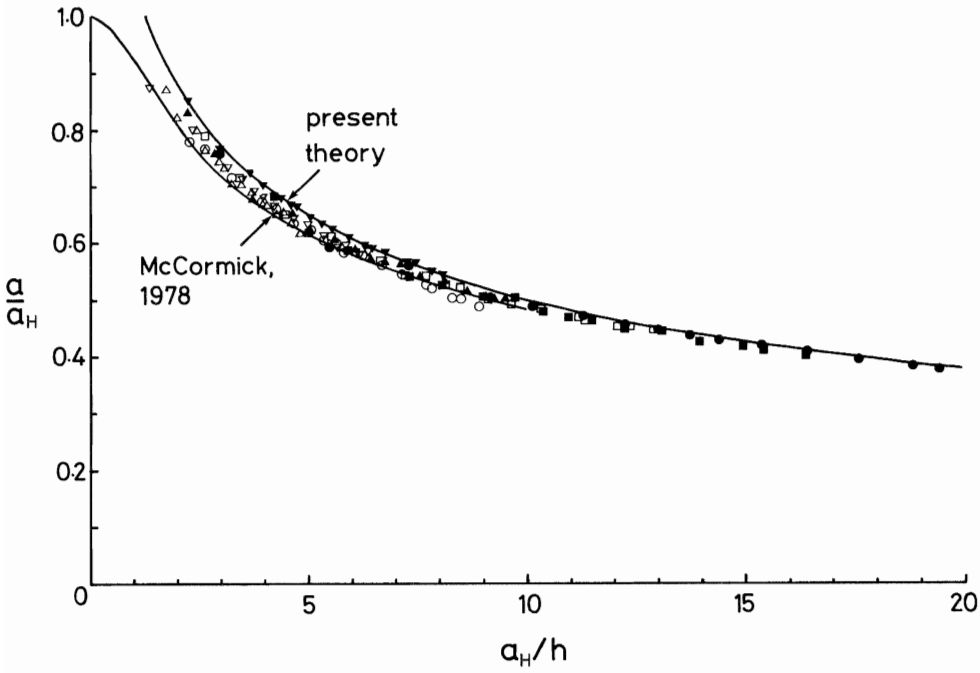

FIG. 9. Indentation by a sphere. Variation of a/a_H with a_H/h for $\nu = 0{\cdot}5$. For key to symbols, see Table 1.

TABLE 1. *Key to symbols of Fig. 9*

	G (kPa)	R (mm)	h (mm)
●	310	400	1·15
■	310	200	1·15
▲	310	47	1·15
▼	89	47	2·15
○	110	15	1·30
□	110	47	1·30
△	300	15	1·81
▽	300	47	1·81

3.2 *Indentation by cones*

The contact radius has been measured as a function of load when a cone is loaded onto the coating. Typical results are shown in Fig. 11. The theory-line is calculated for the measured values of $G = 310$ kPa, $h = 1{\cdot}15$ mm and $\theta = 84{\cdot}5°$, and for $\nu = \frac{1}{2}$. Some systematic deviation of the theory from experiment is shown. Figure 12 shows the predicted behaviour of the dimensionless load

$$P^* = \frac{P \tan \theta}{2\pi a^2 G}$$

as a function of a/h. This line represents a "master-curve" for elastomeric coating materials. Superimposed are data from a number of experiments. The theory deviates

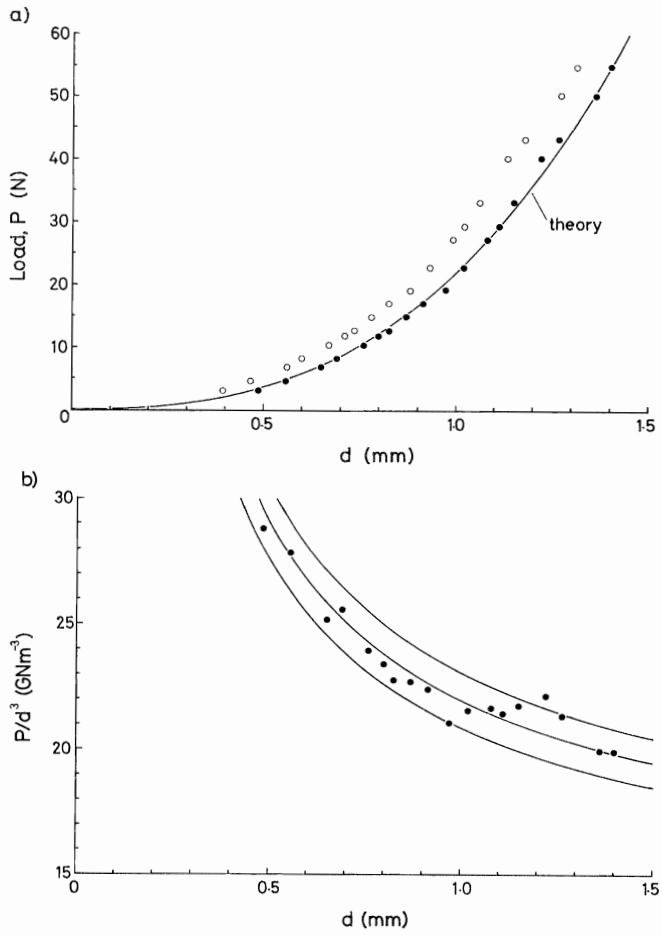

FIG. 10. Indentation by a sphere. (a) Variation of load P with penetration d. The open circles are the data as measured and the closed circles are these data with an offset of 90 μm on the penetration. The theory-line is calculated using the measured values $G = 24$ kPa, $R = 47$ mm, $h = 2{\cdot}88$ mm and $\nu = 0{\cdot}5$. (b) Results of (a) replotted as P/d^3 vs d. The three theory-lines are calculated using the measured value of the modulus and this value plus and minus the error of 5%.

systematically from data from all experiments. However, the theory ignores the rapidly changing, and large, stresses near the tip of the cone and some error is to be expected. The predictions of the theory, albeit limited, are of use as they are well within an order-of-magnitude accuracy. A more precise solution for conical indentation can be expected to be considerably more complicated than that provided by the present theory.

4. Discussion and Conclusions

An analysis has been developed which describes the axi-symmetric contact on a coating by an indenter of general cross-section. The assumptions that the coating is thin and the indenter is large enable certain approximations to be made which

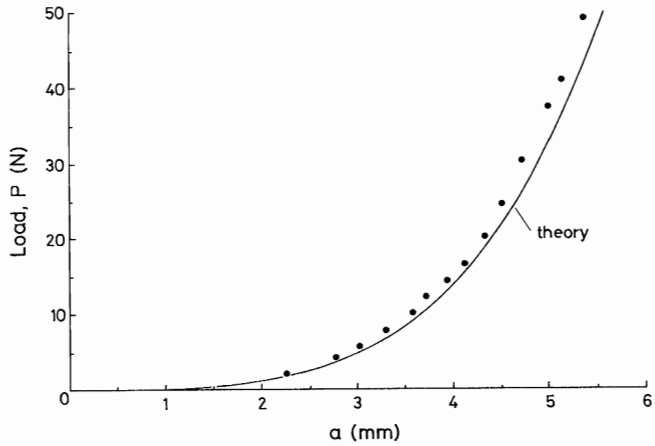

FIG. 11. Indentation by a cone. Load P vs contact radius a. Theory-line calculated for $G = 310$ kPa, $\theta = 84{\cdot}5°$, $h = 1{\cdot}15$ mm and $\nu = \frac{1}{2}$.

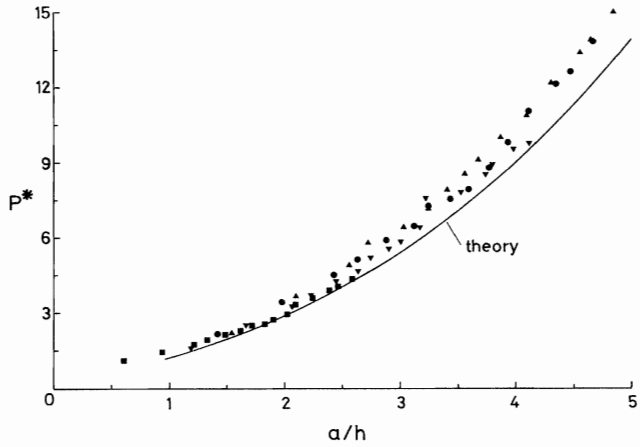

FIG. 12. Indentation by a cone. Dimensionless load P^* as a function of a/h. $\nu = \frac{1}{2}$, $\theta = 84{\cdot}5°$.

TABLE 2. *Key to symbols of Fig.* 12

Key	G (kPa)	h (mm)
●	310	1·15
■	34	3·50
▲	260	1·14
▼	270	1·70

simplify the analysis considerably. The solutions for spherical and conical indenters have been obtained explicitly. The stress distributions within the coating have been found and are shown to be extremely sensitive to the Poisson's ratio of the coating. It is of particular interest that the interfacial shear stress between the coating and substrate is largest for almost incompressible materials, and therefore these materials are more likely to debond than others. This is of practical significance. Elastomeric materials have found a wide use for protecting components from impact damage; for

example, vulnerable aircraft components are frequently coated to minimize damage caused by rain or dust impact [see, for example, FYALL (1970) and SCHMITT (1979)]. Elastomers are successful partly because of their large strain-to-fracture and resulting ability to absorb large amounts of the impact energy in elastic deformation. However, these materials are inherently weak and are themselves reinforced by adhesion to the substrate which reduces the strains in the coating which would otherwise be large. If adhesion is lost they are rapidly eroded with a resulting loss of protection. Good adhesion is therefore essential for the optimum performance of any compliant protective coating.

The present analysis can be used to predict properties and minimum useful thickness of coatings required in various situations. MATTHEWSON (1979) has determined the Hertz-like radial tensile stresses in the substrate surface, and he shows that for a well-adhering elastomeric coating they are small and by suitable choice of coating thickness may be made predominantly compressive—suggesting a minimum thickness criterion. Using values of parameters typical of the circumstance of rain erosion, the predicted minimum thickness is found to be $\approx 0{\cdot}3$ mm and compares well with the values 0·2–0·3 mm used in practice on aircraft components (SCHMITT, 1979). In new practical situations, the present theory should allow suitable materials to be chosen much more quickly and efficiently.

The accuracy of the analysis increases with increasing ratio of contact radius to coating thickness and is typically less than 5% which is acceptable for most engineering purposes. The theory shows good agreement with experiments using both spherical and conical indenters and also with McCormick's theory. Although the theory presented here is less accurate than McCormick's and does not cover such a wide range of coating thickness and modulus, it does have the valuable advantage that the results are analytical and can be expressed in closed form and can easily be calculated without the use of special computational techniques. Also, the stress and strain distributions are readily accessible. The analysis provides a useful way of non-destructively measuring the coating modulus *in situ*. The accuracy of the measurement is only limited by the accuracy of the analysis. However, the error in the analysis is systematic and so quite small changes in elastic modulus can be resolved by an indentation technique using this theory.

ACKNOWLEDGEMENTS

I thank Dr. J. E. Field for supervising this work. I am indebted to Professor K. L. Johnson and Dr. J. A. Greenwood (Department of Engineering, University of Cambridge) for useful discussions and helpful suggestions during the course of this work. I also thank the Ministry of Defence (Procurement Executive), Churchill College, Cambridge and the Science Research Council for financial support.

REFERENCES

ABRAMOWITZ, M. and STEGUN, I. E. 1965 *Handbook of Mathematical Functions,* p. 374. Dover, New York.

ALEKSANDROV, V. M. 1962 *J. Math. Mech.* (*PMM*) **26,** 1410.

ALEKSANDROV, V. M. and VOROVICH, I. I.	1964	*Ibid.* **28,** 425.
FYALL, A. A.	1970	*Radome Engineering Handbook* (edited by J. D. Walton), p. 461. Marcel Dekker, New York.
HANNAH, M.	1951	*J. Mech. appl. Math.* ***IV,*** 94.
MATTHEWSON, M. J.	1979	*Proceedings of the 5th International Conference on Erosion by Liquid and Solid Impact* (edited by J. E. Field) (Cambridge. 3–6 September 1979), paper 73. Cavendish Laboratory, University of Cambridge.
MCCORMICK, J. A.	1978	*A numerical solution for a generalised elliptical contact of layered elastic solids.* MTI Report No. 78TR52, Mechanical Technology, Latham, New York.
SCHMITT, G. F.	1979	*Liquid and solid particle impact erosion.* Technical Report AFML–TR–79–4122, Air Force Materials Laboratory, Wright–Patterson Air Force Base, Ohio.
SNEDDON, I. N.	1951	*Fourier Transforms,* pp. 450–510. McGraw–Hill, New York.